Bio-Radar Performance Evaluation for Different Antenna Designs

Carolina Gouveia[1], Daniel Malafaia[1], José N. Vieira[1,2], and Pedro Pinho[1,3]

[1]IT - Instituto de Telecomunicações
Campus Universitário de Santiago
Aveiro, Portugal

[2]IEETA - Instituto de Engenharia Electrónica e Telemática de Aveiro
Campus Universitário de Santiago
Aveiro, Portugal

[3]ISEL - Instituto Superior de Engenharia de Lisboa R. Conselheiro Emídio Navarro 1
Lisboa, Portugal

E-mails: carolina.gouveia@ua.pt, danielmalafaia@ua.pt, jnvieira@ua.pt, ppinho@deetc.isel.pt

Abstract

Cardiopulmonary monitoring without any physical contact with the human body has several applications, such as health monitoring of bedridden patients, monitoring sleeping, or even for rescuing people from collapsed buildings. The Bio-Radar system can accurately measure vital signals by using the principle of the Doppler effect, which relates the properties of the received signal to the distance change between the radar antennas and the person's chest wall. In this paper, a mathematical model of the Bio-Radar is presented. The algorithm used for extracting breathing rate is explained, and an analysis of the influence of the radiation pattern of the antenna on the quality of the received signal is presented. Moreover, we show that an antenna with a narrow beam leads to a better signal-to-noise ratio (SNR). The full performance of the developed prototype was also evaluated by using a certified measuring system to monitor vital signals simultaneously with the Bio-Radar. The signals extracted using both acquisition methods are presented, and a comparison is made in order to prove the accuracy of the prototype.

1. Introduction

Sensor-less measurement of bio-signals has the potential to improve many areas. Among many other applications in the medical field, the continuous monitoring of vital signals in bedridden patients can be highlighted, such as in a burn unit, where physical contact with the patient is discouraged. Other applications include monitoring sleep, to support cases of Obstructive Sleep Apnea Syndrome without interfering with the normal lifestyle of the patients, or in the prevention of Sudden Infant Death Syndrome [1]. In terms of commercial applications, driver monitoring can be highlighted, where the driver's vital signals are monitored to avoid any possible accident in case of cardiac failure. Applications in psychology are also possible, such as, for example, the measurement of stress response [2].

The Bio-Radar system is composed of a continuous-wave Doppler radar that continuously transmits a sinusoidal carrier, generated digitally, and receives the echo from the reflecting target. Due to the Doppler effect, there is a phase change as the subject's chest wall moves towards or away

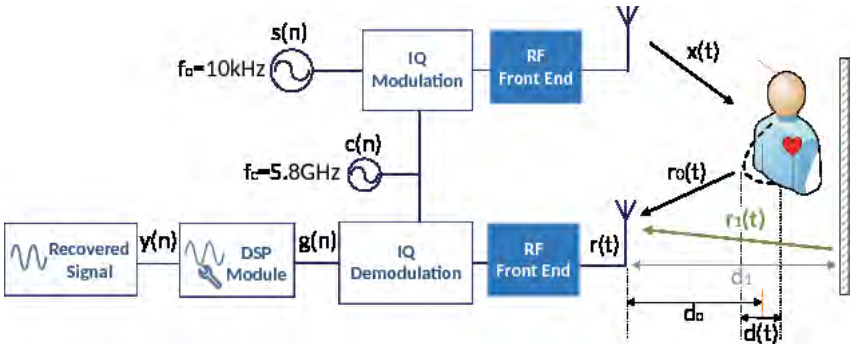

Figure 1. The block diagram of the Bio-Radar system

from the radar, and hence a phase modulation in the received signal is created [3]. The overall system is represented by the block diagram in Figure 1.

The concept of non-contact signal extraction of human physiological parameters was demonstrated by pioneers during the 1970s, where both respiration and heartbeat were separately measured during apnea interspersed periods [4]. Later, between the 1980s and 1990s, this system was implemented using analog and digital signal processing. The state-of-the-art of these systems thus followed a timeline of hardware implementation. The first proposed prototypes were implemented with transceivers composed of single radio-frequency (RF) hardware components interconnected with each other [5]. Later, the RF front-end components were integrated into a single chip using CMOS processes [6]. Nowadays, research in this area is even more focused on the development of systems with features that guarantee low power, small dimensions, better accuracy, long-range detection, and more robust operation. With this in mind, in [7] a bio-radar implementation was proposed using a front-end based on a software-defined radio (SDR) system. These radars allow the digital configuration of the inputs and outputs (receiver and transmitter) with respect to the required frequency and sampling rate of the current application. These configurable systems present an advantage compared to the previously referred-to systems, due to their flexibility and compactness.

Considering the work developed until recent times, the Bio-Radar prototype developed for this work has a front-end based on a software-defined radio and operates in real time, using the *LabVIEW* software. In this way, the acquired signals can be processed and visualized during their acquisition time. In this paper, a mathematical model that synthesizes the Bio-Radar system's behavior is also presented. Bio-signals have low amplitudes, and the modulation that they create on the radar's transmitted signal in baseband will be very close to dc. They hence are highly sensitive to several sources of noise, such as reflections from surrounding objects. The antenna design should therefore guarantee maximum directivity and a narrow beamwidth to focus exclusively on the human chest wall, and to thus avoid the reception of undesired reflections. Experiments were conducted using two antennas with different designs and different carriers. The dc component present in the signal was computed for each experiment, in order to evaluate the impact of the antenna's design on the received signal. Finally, the performance of the proposed Bio-Radar prototype was evaluated by measuring the vital signals of a subject simultaneously with a certified measuring system, called BioPac.

This paper is organized as follows. In the next section, we will start by presenting a mathematical model for the Bio-Radar system. In Section 2.2, we present a description of the extraction of the breathing signal. In Section 3, we present the implementation of the system and some real measurements obtained by the software-defined-radio-based test bed. The main conclusions are finally presented. All the tests conducted were focused on the acquisition of the respiratory signals.

2. Modeling the Bio-Radar System

2.1 Signal Model for the Bio-Radar Channel Response

Regarding the block diagram presented in Figure 1, a baseband signal is digitally generated with a sampling rate f_s. The signal is a complex sinusoid, with frequency ω_0 and amplitude A, and it is represented by

$$s(n) = Ae^{j\omega_0 n}. \tag{1}$$

The signal $s(n)$ is then modulated with in-phase and quadrature (IQ) modulations, with a carrier frequency ω_c This leads to the signal given by Equation (2), which is transmitted towards the target:

$$x(t) = A\cos\left[(\omega_0 + \omega_c)t\right]. \tag{2}$$

The received signal encompasses the time-variant signal $r_0(t)$, corresponding to the chest-wall reflection and the stationary signal, $r_1(t)$, which represents the sum of the total contributions of the reflections from static objects (clutter). The total signal at the receiver's input can be expressed as

$$r(t) = r_0(t) + r_1(t) \tag{3}$$

$$= A_0\cos\left[(\omega_0 + \omega_c)t + \varphi(t)\right] + A_1\cos\left[(\omega_0 + \omega_c)t + \theta_1\right]$$

where A_0 and A_1 are the amplitudes of the received signal from the subject and the clutter, respectively; $\varphi(t)$ is the phase-change function, which contains the respiratory information; and θ_1 is the phase change due to clutter. After its reception, the signal $r(t)$ is IQ demodulated, resulting in Equation (4), and is sampled at the same sampling rate, f_s, as in the transmission channel:

$$g(n) = A_0 e^{j\varphi(n)} + A_1 e^{j\theta_1}, \tag{4}$$

where θ_1 can be expressed as $\theta_1 = 4\pi d_1/\lambda$, considering that the clutter source is located at an equivalent distance d_1 from the radar, and λ is the wavelength.

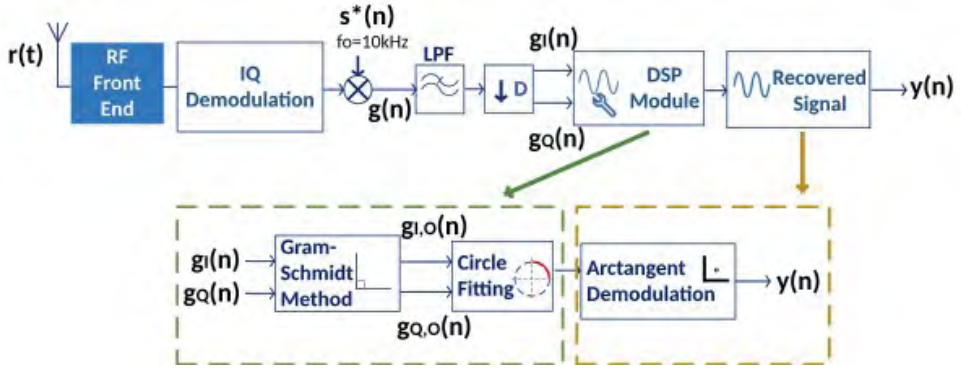

Figure 2. The receiver channel showing the DSP algorithm implementation.

The phase-change function, $\varphi(n)$, results from the chest-wall motion, which changes the distance the wave travels and hence modulates the reflected signal. The phase-change function can this be described by

$$\varphi(n) = \theta_0 + \frac{4\pi d(n)}{\lambda}, \qquad (5)$$

where θ_0 is the phase corresponding to the total path traveled by the wave. This can be expressed as $\theta_0 = (4\pi d_0/\lambda) + \phi$, where d_0 is the nominal distance between the radar and the target, and ϕ is the phase change at the surface of the target. In [8], it was shown that the respiratory signal should be modeled as a half cycle of a sinusoid raised to the *p*th power. However, in the remainder of this work a simpler model is considered, in which the chest movement is described as $d(n) = a_r \cos(2\pi f_1 n)$, where a_r is the amplitude of the chest movement and f_1 is the breathing rate.

2.2 The Extraction Algorithm for the Breathing Signal

Once at baseband, the complex signal $g(n)$ is then processed by the digital signal processing (DSP) algorithm, represented by the block diagram in Figure 2.

The signal $g(n)$ is down-sampled once it is a narrowband low-pass signal, and thus high sampling rates are not needed. The new sampling rate is f_{s2}. For the case of this work, the sampling rates were defined as $f_s = 100$ kHz and $f_{s2} = 100$ Hz.

The phase variation due to the target's motion is represented in the polar plot by an arc (Figure 3a), where the length of the arc is proportional to the amplitude of the respiratory signal, a_r, and the radius of the arc is the received signal's amplitude, A_0.

In an ideal scenario, the arc would fit to a perfect circle centered at zero. However, in real-world scenarios, there is an IQ imbalance effect. This occurs when both the real and imaginary parts do not have the same amplitude, and the phase relationship is not exactly 90°. The arc formed hence becomes an ellipse instead of a circle (Figure 3b). There are also dc offsets present in both the real and imaginary parts of the baseband signal caused by the clutter, which lead to an offset in the arc's center. Figure 3c shows the arc formed with the IQ imbalance effect and the dc offset. These effects should be digitally removed before the phase demodulation in order to guarantee an accurate arctangent result.

The IQ imbalance can be removed by using the Gram-Schmidt method [3, 4] by applying Equation (6),

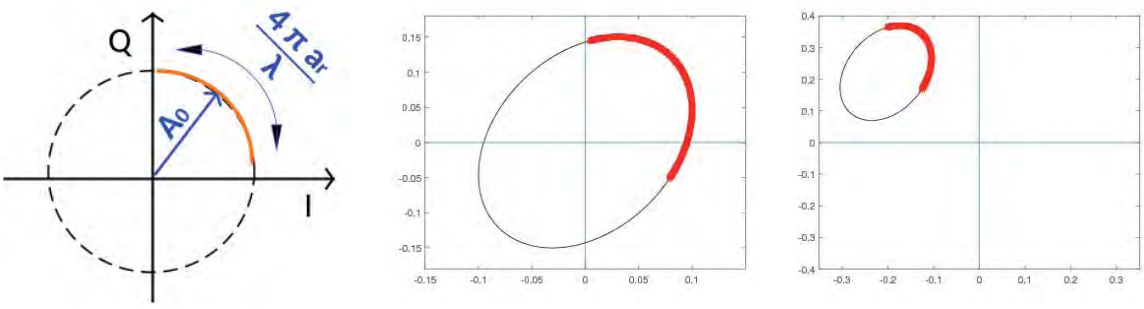

Figure 3. Complex plots of the baseband signal, $g(n)$, due to the target's motion: (a) in an ideal scenario, (b) with the IQ imbalance effect, (c) with a dc offset and the IQ imbalance effect.

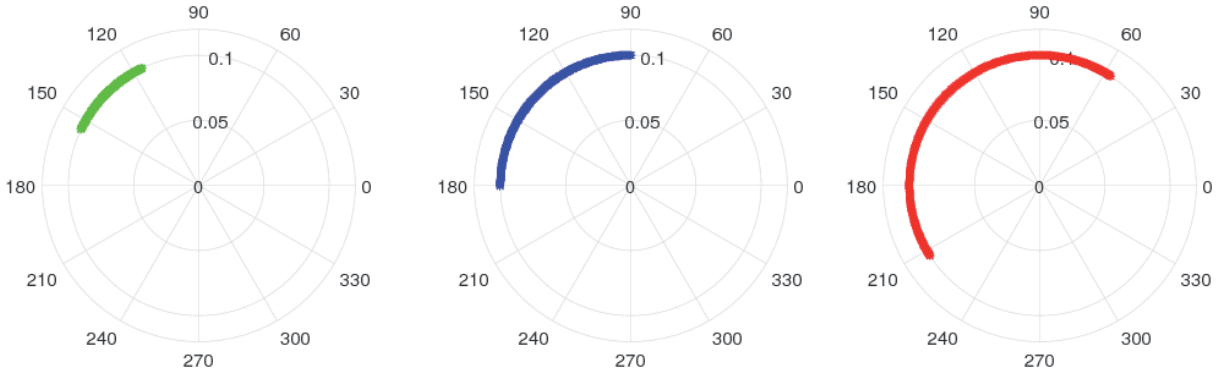

Figure 4. The influence of the carrier frequency, f_c, considering the amplitude of the motion to be $a_r = 0.00325$ for: (a) $f_c = 5.8$ GHz, (b) $f_c = 2.5$ GHz, (c) $f_c = 10$ GHz.

which restores the orthogonality of the baseband signal in quadrature:

$$\begin{bmatrix} g_{I,O}(n) \\ g_{Q,O}(n) \end{bmatrix} = \begin{bmatrix} 1 & 0 \\ -\tan(\psi_E) & \dfrac{1}{A_e \cos(\psi_E)} \end{bmatrix} \begin{bmatrix} g_I(n) \\ g_Q(n) \end{bmatrix} \quad (6)$$

The parameters ψ_E and A_e are the measured phase and amplitude imbalances, respectively; $g_I(n)$ and $g_Q(n)$ are the in-phase and quadrature parts of the baseband signal; and finally, $g_{I,O}(n)$ and $g_{Q,O}(n)$ are the in-phase and quadrature parts with the orthogonality restored. After the imbalance compensation, the dc offsets are estimated and removed using the circle-fitting method [9], which tracks the coordinates of the circle's center, and subtracts them from the complex signal, forcing the arc to be centered at zero. Finally, the arctangent is evaluated in order to extract the respiratory signal [3, 9], obtaining the signal, $y(n)$. From this signal, the respiration rate can be obtained by performing a power-spectrum analysis.

2.3 Carrier Wavelength Impact

The impact of the wavelength was simulated in *MATLAB* and is shown in Figure 4. Different carrier frequencies were used, revealing differences in the arc length.

In [8], it was concluded that the arc length is directly related to the phase modulation. It can be quantified in radians by Equation (7), and the SNR is dependent on the carrier wavelength. Carriers with a higher wavelength thus lead to low SNR, and vice-versa.

$$\Delta\phi = \frac{4\pi\varphi(n)}{\lambda}. \quad (7)$$

Besides the increasing SNR, other advantages in the usage of high frequencies have been identified, for instance, the possibility of using more-compact and portable radar modules, because smaller size antennas can produce the same gain and directivity using higher frequencies. High frequencies also maintain full beam radiating properties for longer distances, and increase the radar cross section of the area of the vital signals [1]. In [10], a study of the optimum carrier frequency in the framework of the detection of bio-signals was made, where the advantages of using the Ka-band were pointed out. Nonetheless, a balance should be reached regarding the increase in frequency. Higher frequencies lead to smaller wavelengths, which eases the detection of signals with low amplitude, such as

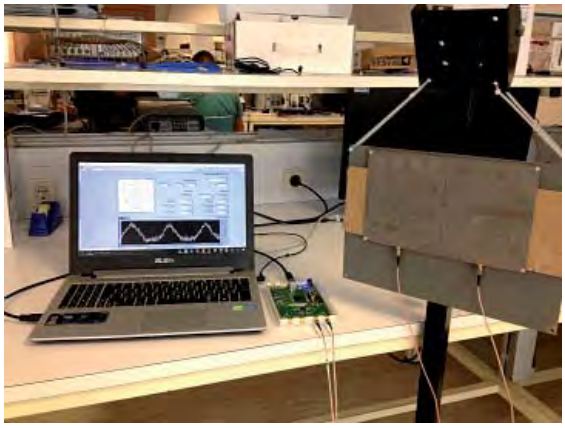

Figure 5. The Bio-Radar prototype, using 5.8 GHz antennas.

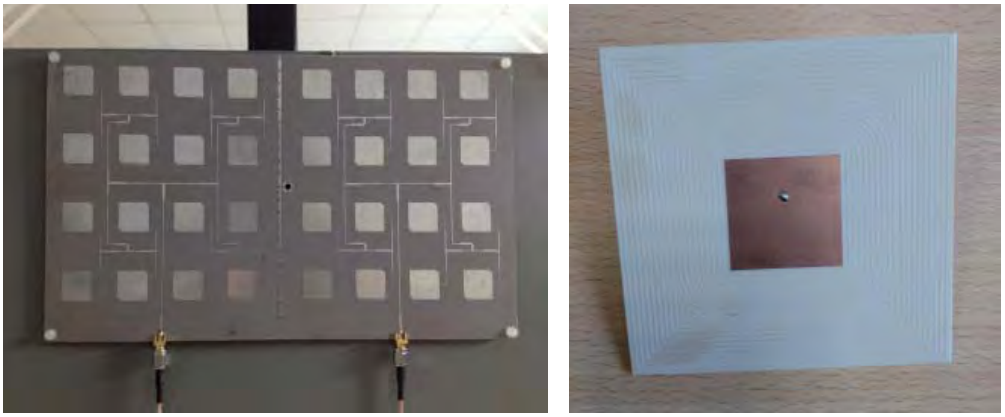

Figure 6. (a) Antenna 1: a 4×4 array of patch antennas at 5.8 GHz, (b) Antenna 2: a single patch of this linear array at 2.5 GHz.

the heartbeat signal. However, when small wavelengths are used, the respiratory signal, $d(n)$, is comparable with the wavelength, and a series of harmonic tones will be produced [1]. This effect can lead to intermodulation between the respiration signal and the heartbeat signal, and can hence hamper the simultaneous measurement of the respiration and heartbeat signals. Furthermore, with lower wavelengths, the arc length is larger, and hence it can easily achieve the full 2π phase rotation in the complex circle [3], causing multiple wraps in the extracted signal.

3. Implementation

The developed Bio-Radar prototype (Figure 5) consisted of a real-time measuring system implemented with the *LabVIEW* software. Signals were acquired using two antennas, one for transmission and the other for reception. The front-end was based on a software-defined radio system, which was a reconfigurable platform that established the connection of the front-end hardware and the DSP software. In the framework of this application, the software-defined radio used was an USRP B210. It digitally did the modulation and demodulation of the RF signals, giving more flexibility on the DSP side. The USRP B210 board operates over a limited range of carriers (70 MHz to 6 GHz). We therefore only used two frequencies: 2.5 GHz and 5.8 GHz.

The experiment conducted was divided into two parts. The goal of the first part was to compare the system's performance with two different types of antennas. Antenna 1 was a 4×4 antenna patch array tuned to a higher frequency, specifically 5.8 GHz. Antenna 2 was a single patch with a frequency of operation equal to 2.5 GHz (see Figure 6). The measured radiation patterns of the antennas are shown in Figure 7, and the magnitudes of the S_{11} values are in Figure 8.

In order to guarantee the same conditions for the experiments with both antennas, the chest-wall simulator (CWS) in Figure 9 was used to emulate the motion of the chest wall at a frequency of 0.4 Hz. For each antenna, the chest-wall simulator's motion was measured twice, at two different nominal distances, for $d_0 = 50$ cm and for $d_0 = 70$ cm. For each experiment, the dc component was measured by computing the absolute value of the signal's mean. The values obtained are discussed in the next section.

The second part of the conducted experiment aimed to validate the prototype's performance. For this purpose, certified measuring equipment, called a Biopac MP100, was

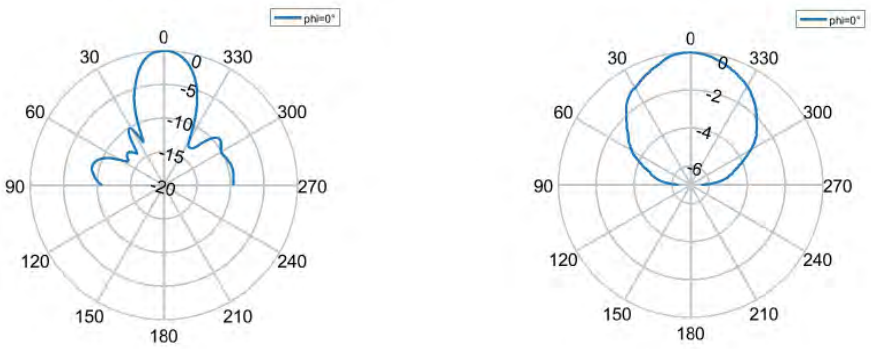

Figure 7. The radiation patterns of the antennas for phi = 0°: (a) antenna 1, (b) antenna 2.

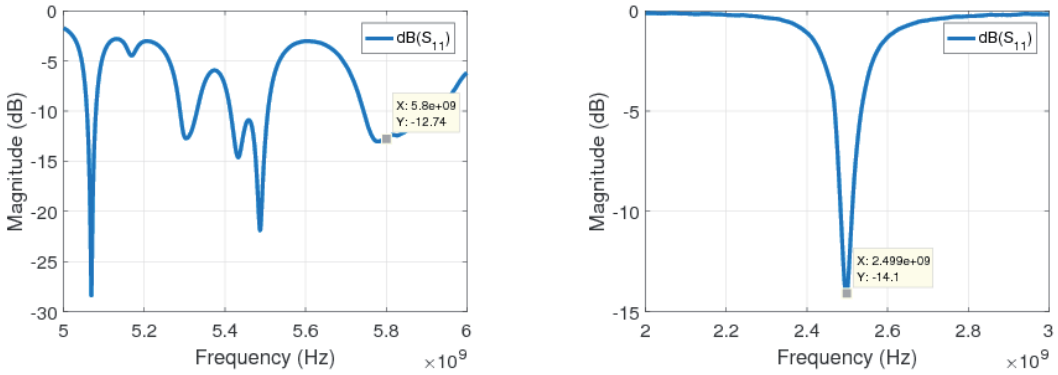

Figure 8. The S_{11} parameter values for (a) antenna 1, (b) antenna 2.

simultaneously used to monitor the vital signals with the Bio-Radar. The Biopac MP100 system was connected to an acquisition board that had several modules for different types of signal acquisition, such as ECG, breathing, and blood pressure. The RSP100C module was focused on the processing of data acquired from a respiration-transducer chest band, TSD201, placed around the chest cavity of the subject in the test. This transducer measured the respiratory effort by analyzing the instantaneous thoracic perimeter. The system set up is shown in Figure 10.

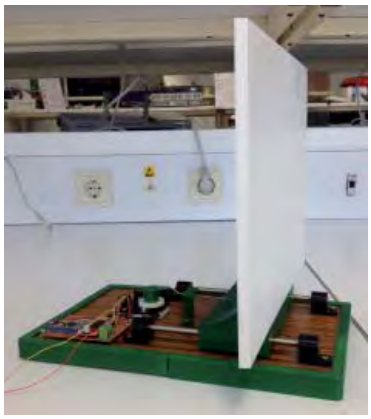

Figure 9. The chest-wall simulator.

A total of three tests were conducted in order to monitor the normal breathing of a healthy volunteer. The subject was seated in front of the Bio-Radar's antennas, with the chest band in place. The subject was asked to stay still while the BioPac and Bio-Radar continuously acquired data. Since it was extremely difficult to start both measuring systems at the same time, an initial breathing pattern (IBP) from the patient was needed as a trigger to establish the beginning of the measurement in order to sync the signals acquired by both the Biopac and the Bio-Radar. The initial breathing pattern was composed of three heavy breaths followed by an apnea period. Figure 11 shows an example of the resultant signal, with the initial breathing pattern and the rest of the measurement. In *MATLAB*, the samples acquired considered for processing were the samples collected during that measuring time (after the initial breathing pattern) labeled as "Normal Breathing" in Figure 11.

The results obtained are presented in the next section, where a comparison is made between the extracted signals acquired by the Bio-Radar and the Biopac.

Table 1. The dc values from the experimental tests.

	$d_0 = 50$ cm	$d_0 = 70$ cm
Antenna 1: 5.8 GHz	0.0115	0.0044
Antenna 2: 2.5 GHz	0.2330	0.2521

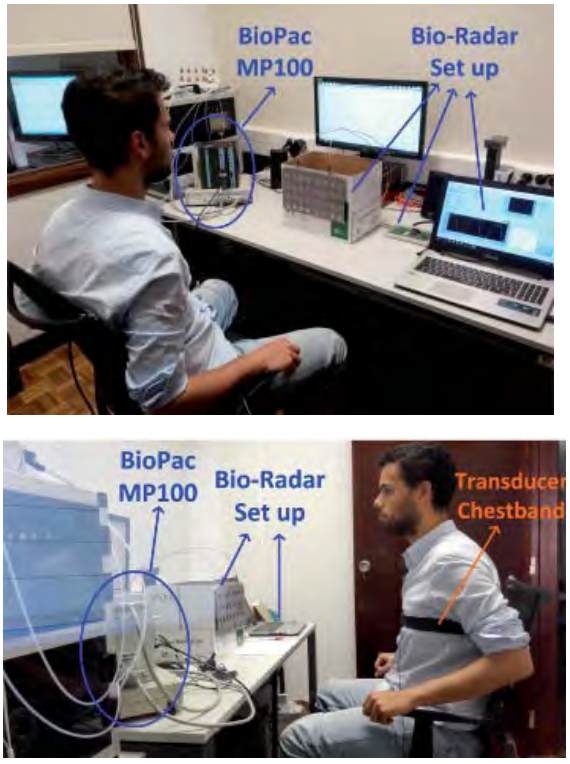

Figure 10. The setup for the conducted tests using the BioPac MP100 and the Bio-Radar: (a) a view of the workbench, (b) a view showing the subject wearing the transducer chest band.

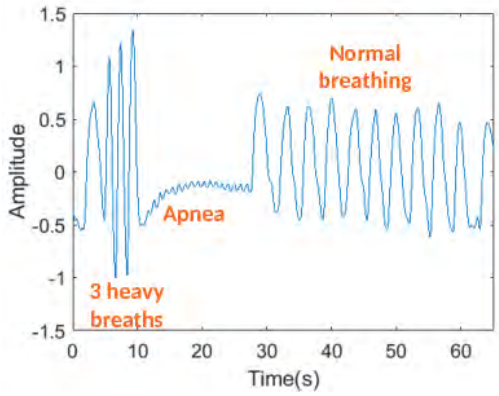

Figure 11. The Biopac signal showing the respiratory pattern (initial breathing pattern, IBP) used for the conducted experiment.

4. Discussion of Results

Regarding the implementation described in the previous section, the discussion of the results is divided in two sections: the influence of the design of the antennas, and the validation of the performance of the full prototype.

4.1 Impact of the Design of the Antennas

Considering the radiation patterns in Figure 7, the half-power beamwidth (HPBW) was computed for each radiation diagram in order to compare the directionality. Antenna 1 presented a half-power beamwidth of 30°, and the half-power beamwidth of antenna 2 was 115°. These results showed that the beam of antenna 1 focused in a specified area reducing the reception of clutter, in contrast with antenna 2, for which in this case more parasitic reflections would be received. This effect is represented by the vectorial diagram of Figure 12.

As previously mentioned, the clutter was perceived as a dc offset, present in both the real and imaginary parts of the signal. This effect was confirmed by the results of the experiments conducted, as presented in Table 1.

The results obtained showed that independently of the target's distance (near to or far from the antennas), antenna 1 presented a lower dc component. In contrast, antenna 2 presented a higher dc component at both testing distances.

Table 2. The respiratory rate for each test using both the Biopac and Bio-Radar, and the center coordinates of the arcs after dc-offset cancellation for the Bio-Radar case.

	Respiratory Rate [Breaths/min]		Arc Center Coordinates	
	Biopac	Bio-Radar	X_{dc}	Y_{dc}
Test 1	17.55	17.55	–4.1021e–18	3.6176e–18
Test 2	18.13	18.13	–2.4369e–17	3.0512e–17
Test 3	14.34	14.93	–1.9019e–18	–6.5228e–18

By implementing the DSP algorithm presented in Section 2.2, the target's motion could be extracted in each test performed, as shown in Figure 13. The signal extracted for antenna 2 had a high presence of noise. To the contrary, the signal from antenna 1 presented significantly less noise. The rate of motion was correctly obtained for both cases (Figure 14 presents the major spectral component at $f_1 = 0.3906$ Hz) regarding the motion frequency of the chest-wall simulator, previously mentioned as 0.4 Hz.

4.2 Bio-Radar Performance Evaluation Using Biopac

Considering the initial breathing pattern used to synchronize both respiratory signals acquired by Bio-Radar and Biopac, their rates were computed using the `pwelch` function from *MATLAB*, and the waveforms obtained were compared. The results are summarized in Table 2. The values of the arc's center coordinates after dc compensation are also presented, once we were dealing with real signals, and thus the DSP algorithm could be also validated.

Comparing the plotted signals from Figure 15, the Bio-Radar and Biopac signals almost totally matched during the proper respiration measurement (after the initial breathing pattern).

The Biopac signal presented a periodic signal with a constant trend, although the signal acquired from the Bio-Radar suffered from some distortion effects due its operating principle. For example, in Figure 15d, a noticeable effect could be observed. In this figure, the Bio-Radar signal

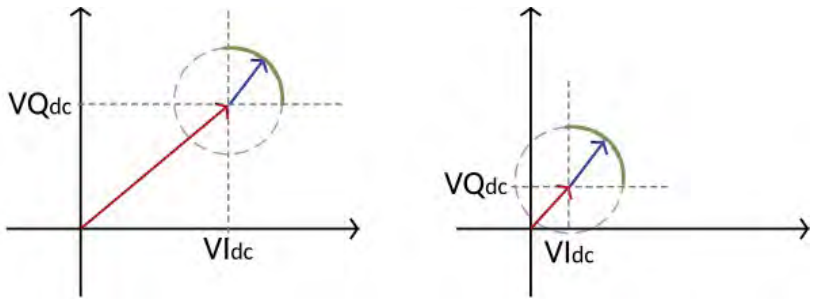

Figure 12. Vectorial diagrams representing the dc components, where the red arrow represents the dc component and the blue arrow represents the signal: (a) For case of non-directive antennas, the dc component is larger than in (b), where a directive antenna was used, and there was less clutter influence.

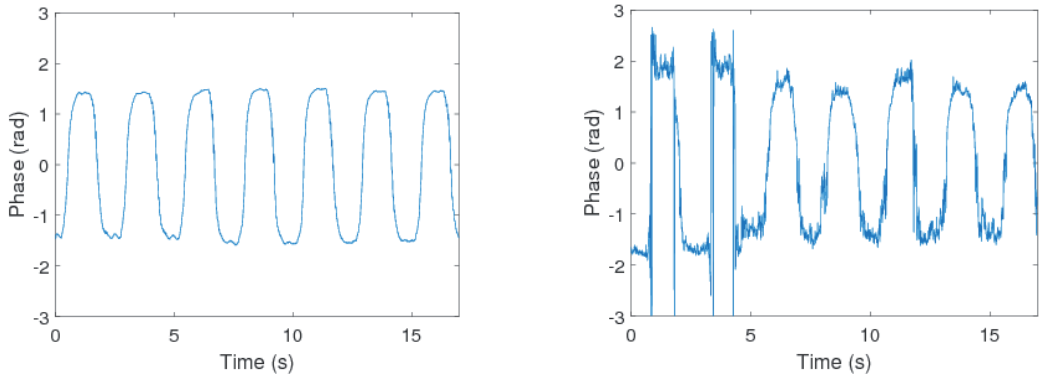

Figure 13. Extraction of the target's motion at a distance of $d_0 = 50$ cm: (a) for antenna 1, (b) for antenna 2.

had a slightly varying mean value. The occurrence of this effect was expected, because the patient did not maintain the same breathing rate and amp Figures 15a, 15c, and 15e represent the signals obtained during the full test, including the initial breathing pattern. The usage of the initial breathing pattern allow providing a visible trigger, and thus, after the apnea period, it was possible to shift the respiratory signal so that it could start at the same instance as the Biopac signal. In these latter figures it was also possible to verify the changed trend in the Bio-Radar signal.

Despite the small effects present in the Bio-Radar signal, it was possible to verify that its extracted signal matched with the Biopac signal.

5. Conclusion

In this work, a mathematical model of the Bio-Radar system was introduced, as well as the DSP algorithm needed for phase demodulation and respiratory signal extraction. The impacts of the design of the antennas and the carrier frequency were also studied. Experimental tests using the chest-wall simulator showed that directive antennas acquired better signals with small dc components and therefore less noise in the signal. However, the narrow beam of antenna 2 implied a better alignment between the antenna and the patient. Finally, the performance of the Bio-Radar in real time and its signal acquisition were validated using the Biopac MP100 measuring system. The Biopac kit acquired the respiratory signal using a transducer chest band located around the thorax of the patient. The signals extracted using both acquisition methods were presented, and a comparison of their computed average rate was made, as well. From the analysis of these, it was possible to conclude that no significant differences were detected, confirming that good performance of the prototype was achieved.

As future work, we intend to design a beamforming antenna with a tracking algorithm to maintain the alignment.

6. Acknowledgement

This work was supported by the European Regional Development Fund (FEDER), through the Competitiveness and Internationalization Operational Programme (COMPETE 2020) of the Portugal 2020 framework

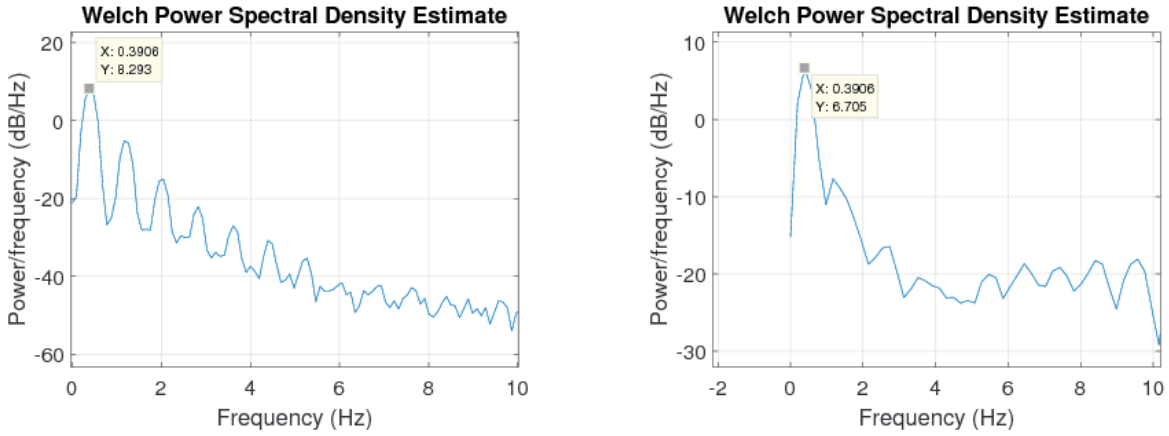

Figure 14. The power spectral density: (a) for antenna 1, (b) for antenna 2.

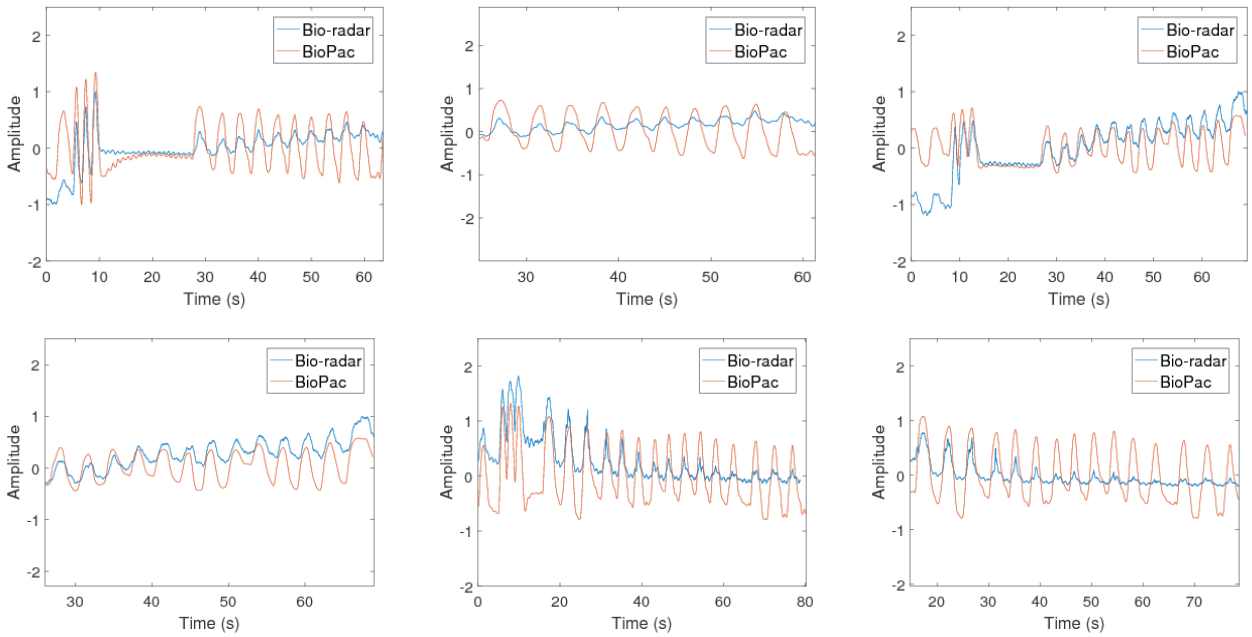

Figure 15. The extracted signal for (respectively) Test 1, Test 2, and Test 3: the signals for the full test are shown in 15a, 15c, and 15e; the extracted respiratory signals are shown in 15b, 15d, and 15f.

[Project TexBoost with Nr. 024523 (POCI-01-0247-FEDER-024523)].

7. References

1. C. Li, V. Lubecke, O. Boric-Lubecke, and J. Lin, "A Review on Recent Advances in Doppler Radar Sensors for Noncontact Healthcare Monitoring," *IEEE Transactions on Microwave Theory and Techniques*, **61**, 5, 2013, pp. 2046-2060.

2. D. Malafaia, et. al., "Cognitive Bio-Radar: The Natural Evolution of Bio-Signals Measurement," *Journal of Medical Systems*, **40**, 10, 2016, p. 219.

3. O. Boric-Lubecke, V. Lubecke, A. Droitcour, B. Park, and A. Singh, *Doppler Radar Physiological Sensing*, New York, John Wiley & Sons, 2015.

4. A. Droitcour, *Non-Contact Measurement of Heart and Respiration Rates with a Single Chip Microwave Doppler Radar*, Doctoral Dissertation, Stanford University, 2006.

5. P. Byung-Kwon, A. Vergara, O. Boric-Lubecke, V. M. Lubecke, and A. Høst-Madsen, "Quadrature Demodulation with DC Cancellation for a Doppler Radar Motion Detector," *IEEE Transactions on Microwave Theory and Techniques*, 2007.

6. C. Li, X. Yu, C. M. Lee, D. Li, L. Ran, and J. Lin, "High Sensitivity Software Configurable 5.8 GHz Radar Sensor Receiver Chip in 0.13 µm CMOS for Non-Contact Vital Sign Detection," *IEEE Transactions on Microwave Theory and Techniques*, **58**, 5, 2010, pp. 1410-1419.

7. D. Malafaia, J. Vieira, and A. Tomé, "Improving Performance of Bio-Radars for Remote Heartbeat and Breathing Detection by using Cyclostationary Features," Proceedings of the International Joint Conference on Biomedical Engineering Systems and Technologies, **4**, pp. 344-349.

8. M. Zakrzewski, H. Raittinen, and J. Vanhala, "Comparison of Center Estimation Algorithms for Heart and Respiration Monitoring with Microwave Doppler Radar," *IEEE Sensors Journal*, **12**, 3, 2012, pp. 627-634.

9. B. Park, V. Lubecke, O. Boric-Lubecke, and A. Høst-Madsen, "Center Tracking Quadrature Demodulation for a Doppler Radar Motion Detector," Microwave Symposium IEEE/MTT-S International, 2007, pp. 1323-1326.

10. C. Li and J. Lin, "Optimal Carrier Frequency of Non-Contact Vital Sign Detectors," IEEE Radio and Wireless Symposium, 2007, pp. 281-284.